Available online at www.sciencedirect.com
SCIENCE DIRECT®
International Journal of Heat and Mass Transfer 47 (2004) 2379–2393
International Journal of HEAT and MASS TRANSFER
www.elsevier.com/locate/ijhmt

On heat transfer enhancement in swirl pipe flows

S. Martemianov [a,*], V.L. Okulov [a,b]

[a] Laboratoire d'Etudes Thermiques UMR CNRS 6608, ESIP, 40 Avenue du Recteur Pineau, 68022 Poitiers Cedex, France
[b] Institute of Thermophysics, Lavrentyev Ave. 1, 630090 Novosibirsk, Russia

Received 13 June 2003

Abstract

We propose theoretical model of the heat transfer in the axisymmetric swirl pipe flows. The model is used to study influences of the type of vortex symmetry and of the vorticity distribution in the vortex core on the heat transfer enhancement.

The study shows that traditional empirical correlations for swirl flows are, in general, insufficient. Indeed, two types of vortex structures can exist in the swirl flows with the same integral characteristics: vortices with left-handed and right-handed helical symmetry. Left-handed helical vortexes generate wake-like swirl flows and increase heat transfer in comparison with the axial flow. Right-handed vortex structures generate jet-like swirl flows and can diminish heat transfer.

Two major factors of the heat transfer enhancement have been identified: (i) formation of the swirl flow with left-handed helical vortex; (ii) modification of the near wall velocity profile of the inviscid flow due to the different vorticity distribution in the vortex core.

1. Introduction

Swirl flows have wide range of applications in various engineering areas such as chemical and mechanical mixing and separation devices, combustion chambers, turbo machinery, rocketry, fusion reactors, pollution control devices, etc. Better utilization of swirl flows may lead to the heat and mass transfer enhancements. Problems of heat and mass transfer in swirl pipe flows are of practical importance in designing different heat and mass transfer exchangers, submerged burners, heat transfer promoters and chemical reactors.

Swirl flows result from an application of a spiral motion, a swirl velocity component (also called as "tangential" or "azimuthal" velocity component) being imparted to the flow by the use of various swirl-generating methods [1]. Many researchers have studied heat transfer characteristics of swirl flows using different swirl generators: axial blades placed in the pipe inlet region [2]; short length helical inserts [3]; tangential injector [4,5]; tangential vane swirl generators [6,7]; radial blade cascade [8], etc. These studies show essential distinction in influence of different swirlers on the heat transfer characteristics. Experimental data [9–12] also show a different influence of swirlers on the mass transfer characteristics in annular and cylindrical tubes.

Usually the swirling pipe flows are classified into two types: (i) continuous swirl flows, which maintain their characteristics over entire length of test section; and (ii) decaying swirl flows. Additional difference in properties of swirl flows is related with the rate of swirl intensity, see for example [13]. This traditional classification of swirl flows is not sufficient for explanation of the heat and mass transfer in swirl flows. From the hydrodynamic point of view, the major problem is an incomplete understanding of the swirl flow parameters. Swirl flow is usually referred to a vortex structure with a central vortex core and an axial velocity component. Recent progress in study of these vortex structures reveals the direct relation between the type of vortex symmetry (left- or right-handed symmetry) and the appearance of swirl flows with jet-like or wake-like

* Corresponding author. Tel.: +33-5-49-45-39-04; fax: +33-5-49-45-35-39.
E-mail address: martemianov@esip.univ-poitiers.fr (S. Martemianov).

0017-9310/$ - see front matter © 2003 Elsevier Ltd. All rights reserved.
doi:10.1016/j.ijheatmasstransfer.2003.11.005

Nomenclature

a, b, c	empirical constants
E	axial flux of energy (kg m^2/s), dimensionless parameter: $E/\rho U^3 R^2$
G	flow circulation (m^2/s), dimensionless parameter: G/RU
J	axial flux of momentum (kg m/s), dimensionless parameter: $J/\rho U^2 R^2$
k	mass transfer coefficient on the wall (m/s)
$l \cdot (2\pi)$	pitch of vortex lines (m), dimensionless parameter: l/R
L	length of a cylindrical mass transfer section (m)
M	axial flux of angular momentum (kg m^2/s^2), dimensionless parameter: $M/\rho U^2 R^3$
Nu	Nusselt number
Nu_0	Nusselt number in non-swirl flow
p	pressure (kg m/s^2), dimensionless parameter: $p/\rho U^2$
p_0	static pressure in the system (kg m/s^2), dimensionless parameter: $p_0/\rho U^2$
R	radius of a cylindrical mass transfer section, $d_h/2$ (m)
Re	Reynolds number
Q	volumetric flow rate (kg/s), dimensionless parameter: $Q/\rho U R^2$
Sc	Schmidt number
S	swirl number
S^*	design swirl number
Sh	Sherwood number
U	mean axial velocity, Q/Σ (m/s)
V	tangential velocity of inviscid flow on a wall, $\equiv w_\varphi(R)$ (m/s)
w_0	velocity on a flow axis (m/s), dimensionless parameter: w_0/U
W	axial velocity of inviscid flow on a wall, $\equiv w_z(R)$ (m/s)
(r, φ, z)	cylindrical coordinate system in inviscid flow (m, rad, m)
z	coordinate oriented along the flow (m)
$(0, w_\varphi, w_z)$	velocity components of inviscid flow (m/s)
$(u_x = u_\varphi; u_y = -u_r; u_z)$	velocity components in boundary layer (m/s)
(x, y, z)	coordinate system in boundary layer (m)
y	distance from the wall in the normal direction, $R - r$ (m)
x	coordinate in the tangential direction (m)

Greek symbols

α	empirical constant
Γ	vortex circulation (m^2/s), dimensionless parameters: Γ/RU
δ	diffusion boundary layer thickness (m)
ε	radius of vortex core (m), dimensionless parameter: ε/R
ν	kinematics viscosity of a fluid (m^2/s)
ρ	fluid density (kg/m^3)
τ_φ, τ_z	local shear stress at the tube wall (kg/m s^2)
ω_z	axial component of a vorticity (1/s)
ω_φ	tangential component of a vorticity (1/s)

profile of the axial velocity [14,15]. Both of these types of swirl flows can be continuous or decaying and can have high or low swirl intensity. Further studies [16,17] have shown that, under the same integral flow parameters (flow rate, flow circulation, axial fluxes of momentum, angular momentum and energy), both left-handed and right-handed vortex structures can be realized; there is even a possibility of the transition between different types of symmetry in the same flow.

Another problem is an insufficient description of the vortex structures for laminar and turbulent flow regimes. Vorticity distribution in the vortex core is different for these flow regimes as the diffusion of all passive scalars in turbulent flows is more important then in laminar ones. To authors' knowledge, no data are reported in the literature on an influence of the vorticity distribution in vortex core on the transfer processes in swirl flows.

It is clear that ambiguities in flow regimes lead to heat (or mass) transfer ambiguities. For this reason, the study of the influence of the type of the vortex symmetry and the vorticity distribution in the vortex core on the transfer processes in swirl flows is of great interest. This is the main goal of this paper.

2. Empirical correlating equations in swirl flows and existence of vortices with different vortex symmetry

Traditional form of correlating equation for convective heat transfer is

$$Nu \cdot f(Pr) = aRe_U^b, \tag{2.1}$$

where a and power factor b are empirical constants. In (2.1) Reynolds number Re_U, calculated via average flow rate velocity U, is usually used as a universal similarity parameter to identify a flow influence on the heat transfer processes. Some authors directly use Eq. (2.1) to predict transfer processes in swirl flows (see for example [6]). However, an additional hydrodynamic parameter,

the swirl number, is usually introduced to describe transfer processes in the swirl flows. This parameter characterizes the rate of flow swirling.

The definition of the swirl number varies from author to author. The complete form of its definition for pipe flow is [1]

$$S = M/JR. \tag{2.2}$$

Here $M = \int_\Sigma \rho w_\varphi w_z r \,\mathrm{d}\Sigma$ and $J = \int_\Sigma (p + \rho w_z^2)\,\mathrm{d}\Sigma$ are the axial components of the flux of angular momentum and momentum, w_z and w_φ are the axial and tangential velocity components, r is the radial coordinate, ρ is the fluid density, R is the pipe radius, p is the pressure, Σ is the pipe cross-section. The turbulent fluctuations are generally neglected, therefore the pressure and velocities are considered to be time-averaged. An exact calculation of the swirl number by means of Eq. (2.2) is practically impossible since the velocity and the pressure fields are usually unknown. The widespread simplification of the definition of the swirl number is given by the formula:

$$S^* = \int_0^R w_\varphi w_z r^2 \,\mathrm{d}r \Big/ \left(R \cdot \int_0^R w_z^2 r \,\mathrm{d}r \right). \tag{2.3}$$

However, in the practical studies and engineering applications the swirl number is replaced by simpler parameter, so-called design swirl number. There are various ways of determining this parameter. Simplest possibility is to identify the design swirl number $S_{V/W}$ with the ratio of maximum (or average) tangential velocity to a maximum (or average) axial velocity (see for example [19]). Another possibility is to evaluate swirl number through the geometric parameters of a vortex chamber. In [7,12] an angle θ between the swirler vane and the pipe axis was used as the design swirl number.

There were many prior attempts to describe heat (or mass) transfer in the swirl flows. To our knowledge, these attempts were restricted to determination of empirical correlating equations with different definition of the swirl number. In the recent works on heat transfer in the air swirl flows generated by different radial guide vane swirlers [7] or snail swirlers [20] the following correlations were proposed:

$$Nu \cdot Pr^{-0.4} = aRe^b(1 + \tan\theta)^c, \tag{2.4}$$

where θ is an angle between swirler vane and pipe axis which can be interpreted as the design swirl number; and a, b, c are different empirical constants. Similar correlation was obtained previously by [12] for mass transfer:

$$Sh \cdot Sc^{-1/3} = aRe^b(1 + \tan\theta)^c. \tag{2.5}$$

In experiments described in [4], the air was injected through six tangential injectors placed on the pipe periphery. Authors used the reduced form of the swirl number (2.3) in the correlation equation:

$$\frac{Nu}{Nu_0} - 1 = a(S^*)^b, \tag{2.6}$$

where Nu_0 is Nusselt number in laminar non-swirl flow. In theoretical studies of [19,21] the resulting formula for Nusselt number was presented via the simplest form of the swirl number $S_{V/W}$:

$$Nu \cdot Pr^{-0.4} = a\left[(1 + S_{V/W}^2)^{1/2} Re\right]^b. \tag{2.7}$$

Eqs. (2.4)–(2.7) and ones similar to them postulate that only two parameters, namely Reynolds (Re) and swirl (S) numbers, are essential for the description of the hydrodynamic influence on the heat (or mass) transfer processes in swirl flows. However, in contrast to axial non-swirling flows where one type of the correlating Eq. (2.1) successfully fits experimental data, for swirl flows there are no correlations of a general character. At present, there is no generalized method for prediction of the heat transfer in the swirl flows from known inlet flow conditions that can be applied to different swirl generators. Description of swirl flows only by the means of Reynolds and swirl numbers meets with numerous difficulties. One of the problems deals with the existence of a spontaneous change in flow regimes (see, for example, [22,23]) and with the change of the flow regimes during vortex breakdown [16,17]. In reality, Reynolds and swirl numbers do not determine the only one regime of swirl flow. For example, four different flow regimes were observed in [15] in the same set-up for identical Reynolds and swirl numbers. This phenomenon can be related with the appearance in the flow of the large-scale vortices having various structures (their classification is given in [15]). The origin of these ambiguities is related to the existence of different types of vortex symmetry.

Below we use an example of the simplest axisymmetric swirl flow for demonstration of the differences between flow regimes induced by vortices with different helical symmetry. Let vortex axis coincides with the pipe axis, the vortex core has the radius $\varepsilon < R$ (Fig. 1). We suppose that the vortex core has a circulation Γ and consists from helical vortex lines with a constant pitch—$2\pi l$. In other words, components of the vorticity in the axisymmetric vortex with helical symmetry satisfy following relations:

$$\omega_\varphi/\omega_z = r/l \quad \text{and} \quad \omega_r = 0.$$

In this section we consider a simple example of the vortex core with a constant axial component of the vorticity in the cross-section:

$$\omega_z = \frac{2\Gamma}{\varepsilon^2} \begin{cases} 1 & \text{when } r < \varepsilon, \\ 0 & \text{when } r \geqslant \varepsilon. \end{cases} \tag{2.8}$$

This vortex core induces the inviscid velocity field, which is the exact solution of Euler equations [24]:

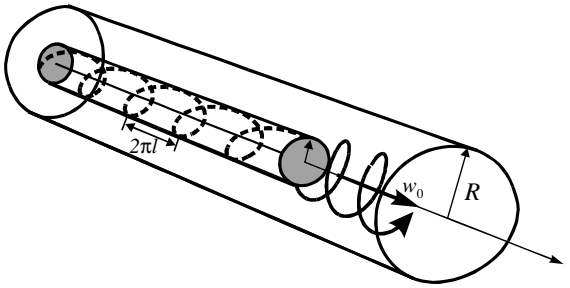

Fig. 1. Swirl flow in a tube generated by an axisymmetric helical vortex structure: *dashed line*—shape of helical vortex lines forming the vortex core; ε—radius of the core; *solid line*—trajectory of fluid motion.

$$w_\varphi = \frac{\Gamma}{r} f(r,\varepsilon), \quad w_z = w_0 - \frac{\Gamma}{l} f(r,\varepsilon),$$
$$\text{where } f(r,\varepsilon) = \begin{cases} r^2/\varepsilon^2 & \text{when } r < \varepsilon, \\ 1 & \text{when } r \geqslant \varepsilon. \end{cases} \tag{2.9}$$

Here w_0 is the velocity on the flow axis (Fig. 1). It was shown that Eq. (2.9) gives a good approximation of an experimental data for various swirl flows [15,16,25]. For this reason, the flows described by Eqs. (2.8) and (2.9) may be considered as the good approximations for the flow core in the inlet of swirl pipe flow. In some sense the velocity distributions given by Eqs. (2.8) and (2.9) play for the inlet swirl pipe flow the same role as a step-shape profile approximation for the inlet non-swirl pipe flow.

The swirl flow induced by the step-shape distribution of the vorticity, Eq. (2.8), has a set of axial velocity profiles under the same Reynolds and swirl numbers, see Fig. 2. This is the main distinction between flows with and without swirling. When the pitch l between the vortex lines is equal to infinity, vortex described by Eq. (2.9) is equivalent to the well-known Rankine vortex with a uniform profile of the axial velocity. This flow configuration is similar to the one in an inlet non-swirl flow (Fig. 2b). Right-handed helical vortex with positive value of l generates jet-like profile of the axial velocity (Fig. 2c), while left-handed helical vortex with negative value of l generates wake-like profile (Fig. 2d). The last type of vortex can even induce a counter flow in the pipe (Fig. 2e). The fact of existence of right-handed and left-handed helical vortices with the same integral flow parameters was established by theoretical analysis of vortex breakdown [16].

From the practical point of view, the existence of vortices with different vortex symmetry means that traditional parameters, namely Reynolds and swirl numbers, are insufficient for the prediction of the heat and mass transfer in swirl flows. Ambiguities in the flow regimes lead to heat and mass transfer ambiguities. These ambiguities can be very important for heat (or mass) transfer control. In early work [26] the existence of the recirculation zone at the center of the tube (Fig. 2e) has been mentioned as a possible mechanism of heat transfer enhancement in the swirl flows. Indeed, the recirculation zone improves the convective heat transfer because it increases the axial velocity near the wall by reducing the effective cross-section flow area. The increase of the near-wall velocity, in turn, produces larger temperature gradients and higher heat transfer rate. It was shown experimentally [4] that one of the major mechanisms of the heat transfer enhancement is a high axial velocity near the wall. Recently [25] it have been justified theoretically that, under the same flow conditions, mass flux on the wall in swirl flows can decrease or increase in comparison with axial flow. The possible increasing or decreasing in the mass flux is determined by the values of axial velocity near the wall (Fig. 2b–e).

In the following section we reproduce the classical methodology for calculations of the wall heat flux at an inlet of the swirl flow. Our goal is to demonstrate a dominant role of the near wall velocity for the heat transfer enhancement and to obtain a theoretical basis for explanations of above-mentioned ambiguities, related to the existence of the different types of vortex symmetry.

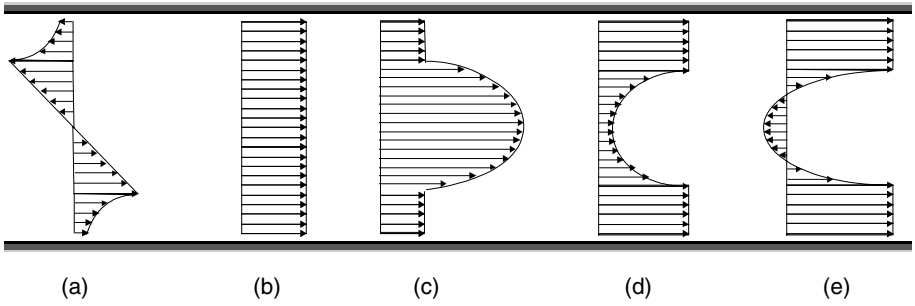

Fig. 2. Possible axial velocity profiles (b)–(e) under the same Reynolds and swirl numbers: (a) tangential velocity profile (the same for all flow regimes); (b) uniform profile generated by Rankine vortex; (c) jet-like profile generated by the right-handed helical vortex; (d) wake-like profile generated by the left-handed helical vortex; (e) wake-like profile with counter flow generated by the left-handed helical vortex.

3. Wall heat flux in the inlet of swirl pipe flows

In this section we calculate the wall heat flux in the inlet of a swirl pipe flow as a function of parameters of inviscid flow core. The traditional laminar boundary layer methodology is used without any empirical hypotheses or "analogy" arguments. We consider the mathematically simple case of a swirl flow in a cylindrical heat transfer section of radius R and length L. The further calculations take into account the following assumptions:

- flow regime is steady and axisymmetric; influence of turbulent pulsations and three-dimensional effects are neglected;
- the heat transfer section is short (flow inlet), so the developing hydrodynamic boundary layer does not essentially influence the inviscid flow core;
- heat transfer does not influence the hydrodynamics;
- curvature of hydrodynamic and thermal boundary layers is small in comparison with the tube radius.

As the boundary layer thickness is small, it is possible to neglect the curvature of the tube and to use a planar coordinate system related to the wall (see Fig. 3).

The near wall velocity profile in the inlet of the tube can be calculated from the 3-D equations for hydrodynamic boundary layer:

$$\begin{cases} u_y\dfrac{\partial u_x}{\partial y}+u_z\dfrac{\partial u_x}{\partial z}=\nu\dfrac{\partial^2 u_x}{\partial y^2}, \\ u_y\dfrac{\partial u_z}{\partial y}+u_z\dfrac{\partial u_z}{\partial z}=\nu\dfrac{\partial^2 u_z}{\partial y^2}-\dfrac{1}{\rho}\dfrac{\partial p}{\partial z}, \\ \dfrac{\partial u_y}{\partial y}+\dfrac{\partial u_z}{\partial z}=0 \end{cases} \tag{3.1}$$

with the following boundary conditions:

$$y=0: \quad u_x=u_y=u_z=0 \quad \text{and}$$
$$y=\infty: \quad u_x=w_\varphi(R)\equiv V, \quad u_z=w_z(R)\equiv W.$$

Here W and V are the axial and tangential velocities components of the inviscid vortex flow core near the wall. The assumption that the flow is axisymmetrical is taken into account in Eqs. (3.1), so all flow characteristics are invariant in the tangential direction (x-axis). It can be noted that Eqs. (3.1) are exactly the same as those obtained for the case of axisymmetrical flow along a body [27].

We assume that friction losses do not influence the inviscid flow core over the entire heat transfer section (this means constancy of the velocities V and W). So, the pressure term in the second equation of (3.1) vanishes, and the first equation of the system (3.1) becomes identical with the second one. Thus, the two velocity components become proportional, exactly as in the case of axisymmetrical flow along a body [27]:

$$\frac{u_x}{u_z}=\frac{u_\varphi}{u_z}=\frac{V}{W}. \tag{3.2}$$

Moreover, the second and the third equations of the system (3.1) become identical with the boundary layer equations for a flat plate. So, the solution of the system (3.1) may be presented in the form:

$$\begin{cases} u_\varphi=u_x=V\phi', \\ -u_r=u_y=\dfrac{1}{2}\sqrt{\dfrac{\nu W}{z}}(\xi\phi'-\phi), \\ u_z=W\phi'. \end{cases} \tag{3.3}$$

Here, the function ϕ is a solution of the Blasius equation [27].

So, we can use the well-known results for a flat plate [27] to calculate Nusselt number in the inlet of an axisymmetric swirl flows:

$$Nu_z/\sqrt{Re}=B(Pr), \tag{3.4}$$

where $Nu_z=q_w(z)\cdot z/\lambda(T_\infty-T_w)$; $Re_z=W\cdot z/\upsilon$; and the function B depends on the thermal boundary condition on the wall. Function B is given for different values of Prandtl number and for different types of boundary conditions (constant temperature or constant heat flux) in [27,28].

The above results are related to the case of heat transfer over the all tube section. In the case when only a

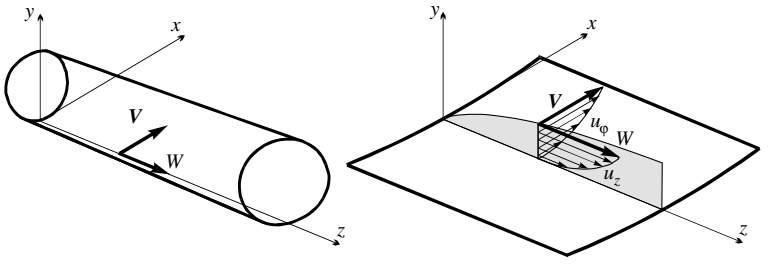

Fig. 3. Coordinate system for three-dimensional boundary layer in a tube.

small part of the tube is heated, the heat flux to the surface is defined by the modulus of the local near wall velocity of the inviscid flow core. For example, if the heated part has a form of a circle with the diameter d_0, we can use result [25], previously obtained for the mass transfer, for the calculation of Nusselt number:

$$Nu = 0.6 \cdot Pr^{1/3} \left(\frac{d_0}{z_0}\right)^{1/6} \cdot \left(\frac{d_0 \cdot (W\sqrt{V^2+W^2})^{1/3}}{\nu}\right)^{1/2}, \tag{3.5}$$

where z_0 is the longitudinal coordinate of the heated spot. Eq. (3.5) is justified for $Pr \gg 1$ and can be used with a good approximation for the case of moderate Prandtl numbers.

Usually Nusselt number in swirl flow is referred to Nusselt number Nu_0 at the axial flow with the same flow rate. If we use this way of presentation, Eqs. (3.4) and (3.5) take the form:

$$\frac{Nu}{Nu_0} = \left(\frac{Re_W}{Re_U}\right)^{1/2} = \left(\frac{W}{U}\right)^{1/2}; \tag{3.6}$$

$$\frac{Nu}{Nu_0} = \left(\frac{Re_{(V,W)}}{Re_U}\right)^{1/2} = \left(\frac{W}{U}\sqrt[3]{\left(1+\frac{V^2}{W^2}\right)}\right)^{1/2}, \tag{3.7}$$

where Reynolds numbers are defined as:

$$Re_W = \frac{d_0 \cdot U}{\nu}; \quad Re_W = \frac{d_0 \cdot W}{\nu};$$

$$Re_{(V,W)} = \frac{d_0 \cdot \sqrt[3]{W(V^2+W^2)}}{\nu}.$$

Eqs. (3.4)–(3.7) show that under the certain conditions (as formulated previously), the wall heat transfer in swirl flows can be predicted as a function of the near wall velocity of the inviscid flow core.

In spite of the simplicity of proposed model, the obtained correlations quite correctly describe variation of heat (mass) transfer coefficients along the pipe surface. The data obtained for the mass transfer coefficient k [12] can be used for verification of (3.5). Fig. 4 shows variation of the mass transfer coefficients $k(z)$, both measured in [12] and calculated (dashed lines) by Eq. (3.5). Initial parts of the curve characterize the flow for the distances up to 5–6 tube diameters from a swirler. It can be noted that Eq. (3.5), after re-adjusting $Re_{w,v}$ parameter, can be successfully applied to describe variation of the mass transfer coefficient not only in the inlet (where the model assumptions are applicable) but also for the developed flow regime (dashed lines in Fig. 4 in the region from 10 to 30 tube diameters).

It is clear that concrete form of correlation equations for Nusselt number can be different from Eqs. (3.4)–(3.7), in particular due to the influence of turbulent pulsations on near wall heat transfer. Nevertheless, it is important that obtained equations explain at least one mechanism of the influence of swirling on the heat transfer. This mechanism is related to the modification of the velocity profile of the inviscid core near the wall. We will show below that, under the same integral flow conditions, near wall velocity can increase or decrease with respect to the axial flow. As a result, we can obtain either enhancement or suppression of the wall heat transfer. This can be a reason of the above-mentioned ambiguities in the transfer processes, which have no explanation in the frame of traditional approach, see Eqs. (2.4)–(2.7).

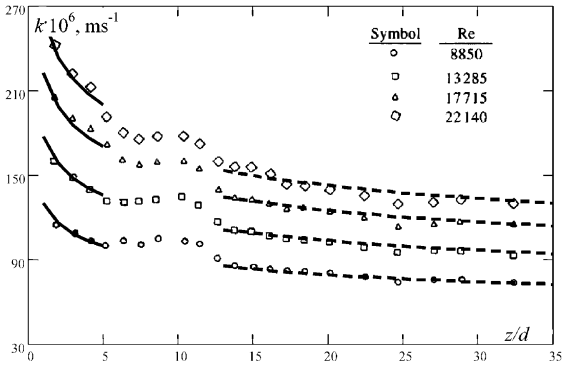

Fig. 4. Variation of mass-transfer coefficients k along the tube in the swirl pipe flow: points—measurements of [4]; lines—calculations by means of Eq. (3.5).

4. Description of swirl flows by means of helical vortex structures with different vorticity distributions in the core

A number of swirlers have been used to generate swirl flow in a tube, including twisted tape inserts, coiled wires, propellers, inlet guided vanes, tangential injection of the fluid, etc. Some of these devices generate swirl continuously along the entire length of the test section; whereas, others are placed at the inlet with the decay of swirl along the tube. In this section, we analyze both types of swirlers using a model of an inviscid flow core induced by helical vortices without losses. The assumption of the existence of helical symmetry is not a fundamental restriction. It was shown previously [15,18,25] that this type of symmetry is realized with a good accuracy in a wide range of flow parameters and for various types of swirlers. The use of a model of an inviscid flow core without losses is a more relevant restriction, which does not allow describing flow transformation along the pipe for decaying swirl flows. However, data of [29] showed that swirl decays to 10–20% only on the length of about 50 diameters. This result was supported by others studies, see for example [4]. It means that estimations of heat

(or mass) transfer both for continuous and for decaying swirl flows may be done with acceptable errors by using a model of an inviscid flow core without losses. This model does not allow estimation of pressure drop characteristics, which are an important parameter for engineering applications. However, the present work has another goal: investigating hydrodynamic possibilities of the heat (or mass) transfer enhancement in the swirl flows.

The step-shape model of the vorticity distribution used in [25] (see Section 2, Eq. (2.8)) is a rather crude model which can be applied only in the inlet of a pipe swirl flow. In all cases, vorticity profile smears along the flow due to the diffusion. That is why the study of the different models of swirl flows, with different approximation of the vorticity distribution in vortex core, is important. Below we shall show that some of these models can be sufficiently used for description of the developed swirl flows with helical symmetry.

Within the frame of the proposed inviscid flow model, it is possible to choose arbitrarily a vorticity distribution in the swirl flow core. Once the helical symmetry is supposed, any distribution of the axial vorticity component acts as an exact solution for Euler equations. Obviously, additional information should be used in order to identify the flow structure. The main goal of this section is to study the legitimacy of different approximations for the vorticity field.

For the axisymmetric helical vortices, equations

$$\begin{aligned} w_\varphi &= \frac{\Gamma}{r} f(r,\varepsilon), \\ w_z &= w_0 - \frac{\Gamma}{l} f(r,\varepsilon), \\ p_z &= p_0 - \rho \Gamma^2 \int_0^r \frac{f(\sigma,\varepsilon)}{\sigma^3} \mathrm{d}\sigma \end{aligned} \tag{4.1}$$

are the solutions of Euler equations [24] for any distribution of the vorticity in the flow core. Here w_φ, w_z are azimuthal and axial velocity components; p is pressure; Γ is the circulation of vortex; ε is its radius; $2\pi l$ is the vortex lines step, w_0 and p_0 are velocity and pressure values at the axis; r is a radial distance from the axis. The function $f(r,\varepsilon)$ determines the vorticity distribution in the flow core.

In addition to the step-shape distribution of vorticity equation (2.8), let us consider below two types of distributions of the axial vorticity component ω_z:

(i) The Gauss distribution, which is equivalent to Lamb vortex with $l \to \infty$ in (4.1):

$$\begin{aligned} \omega_z &= \frac{2\Gamma}{\varepsilon^2} \exp(-r^2/\varepsilon^2), \\ f(r,\varepsilon) &= 1 - \exp(-r^2/\varepsilon^2). \end{aligned} \tag{4.2}$$

(ii) The rational fraction distribution, which is equivalent to Scully vortex with $l \to \infty$ in (4.1):

$$\begin{aligned} \omega_z &= 2\Gamma \frac{\varepsilon^2}{(r^2+\varepsilon^2)^2}, \\ f(r,\varepsilon) &= \frac{r^2}{r^2+\varepsilon^2}. \end{aligned} \tag{4.3}$$

The Gaussian and the rational distributions of the vorticity in the vortex core have been studied in [15,18]. Essential difference between these distributions is related to the fact that the vorticity in the last vortex is less concentrated (see Fig. 9 from [15]). For different flow regimes (laminar or turbulent), we can choose between the two models by correlating the velocity profile Eq. (4.1), obtained for both types of the vorticity distribution, with experimental data of [30–33]. In these works the velocity profiles have been measured at the installations having guide vane swirler with the same geometrical characteristics but different Reynolds number (3220, 4540, 6000, 11 480, 14 100, 20 660, 100 000, 230 000). The results of matching reference flows at low and large Reynolds numbers are shown in Fig. 5. For low Reynolds numbers, the Gaussian distribution fit well the experimental data of [30,31], while at large Reynolds numbers the rational distribution is more suitable approximation for the data obtained by [32,33]. It means that the choice of vorticity distribution depends on the flow regime: Gaussian distribution is more appropriate for the description of laminar swirl flows, while the rational distribution is better adapted for the turbulent ones. This is an expected result: indeed, in turbulent flows the distribution of the vorticity over the tube cross-section should be smoother than in laminar flow due to the turbulent diffusion. This is the case of the rational distribution.

It is interesting to verify if vorticity distributions (4.2) and (4.3) can be useful for description of the velocity profiles generated by different types of swirlers. Gupta et al. [1] classified methods of swirl generation into the three main categories: (i) guide vanes, (ii) tangential entry and (iii) direct rotation. The first type of swirlers has been considered above (see Fig. 5). Below we analyze experimental data obtained for others typical swirlers according to the traditional classification [1]: tangential swirler [4], swirler with combination of axial and tangential entry [34], and swirler with rotating honeycomb section [35]. Comparison of the Gaussian and rational approximations with experimental data for the different swirlers is presented in Figs. 6–8, see also Table 1. Both models fit well experimental data; nevertheless, some difference between the models can be noted. The most important difference between Gaussian and rational models is noted for tangential swirler, Fig. 5. This difference diminishes for tangential and

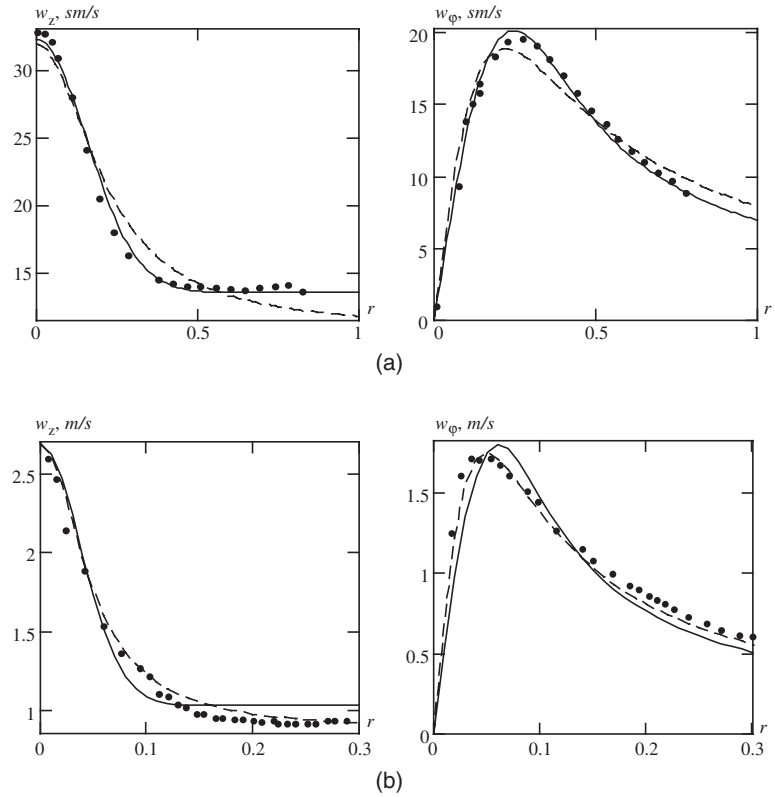

Fig. 5. Comparison of experimental and calculated tangential w_φ and axial w_z velocity profiles: solid lines—Gaussian distribution of the vorticity in the vortex core [18]; dashed lines—rational distribution of the vorticity in the vortex core [18]; points—experimental data at $Re = 11\,480$ (a) [31] and at $Re = 230\,000$ (b) [33].

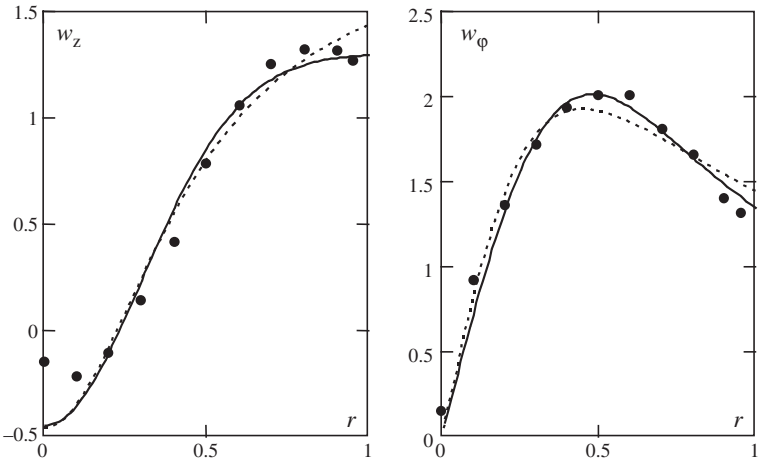

Fig. 6. Pipe swirl flow generated by the tangential swirler: solid lines—Gaussian distribution of the vorticity in the vortex core (present work); dashed lines—rational distribution of the vorticity in the vortex core (present work); points—experimental data [4].

axial–tangential swirlers (Figs. 6 and 7) and becomes negligible for the swirl flow generated by a rotation of honeycomb section (Fig. 8). It is remarkable that the difference between two models is directly related to the type of the vorticity distribution in the core flow (see Fig. 9). For guide vane swirlers the vorticity distribution

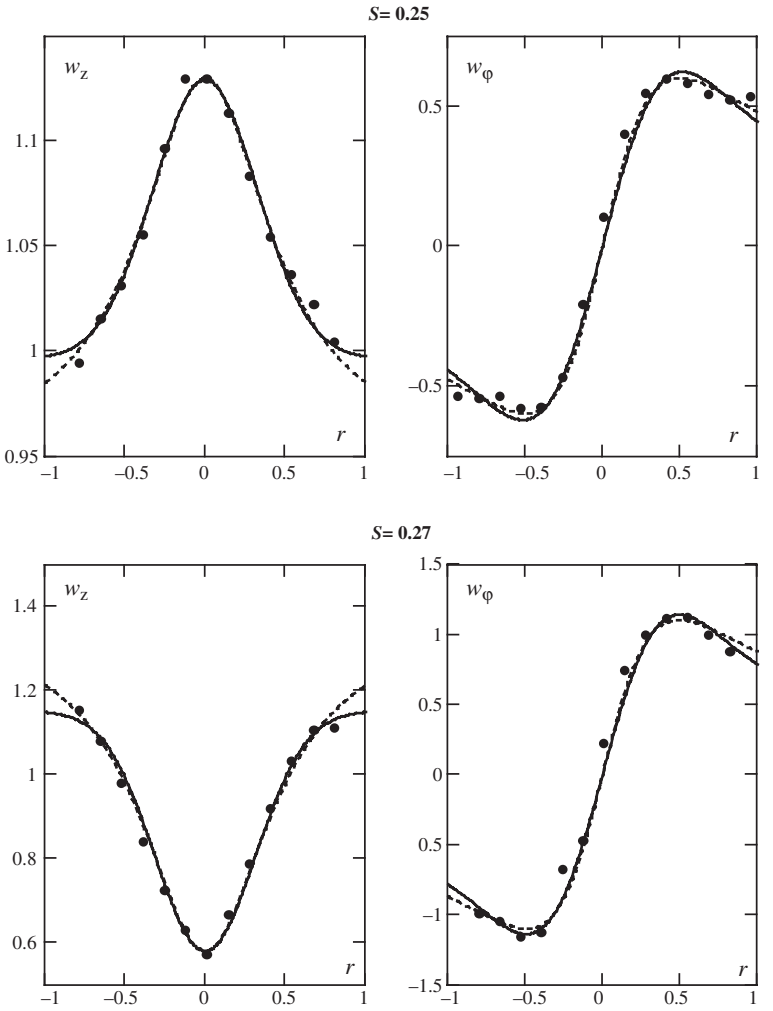

Fig. 7. Pipe swirl flow generated by the axial–tangential inlet: solid lines—Gaussian distribution of the vorticity in the vortex core (present work); dashed lines—rational distribution of the vorticity in the vortex core (present work); points—experimental data [34].

is concentrated near the flow axis (Fig. 9a), and the difference between two models is the most pronounced. For tangential swirlers (Fig. 9b) and swirlers with combination of axial and tangential entry (Fig. 9c) the vorticity distribution is smoother, and the difference between the models diminishes. The last type of swirlers with rotating honeycomb section (Fig. 9d) generates quasi-uniform vorticity distribution, and the difference between the two approximations is negligible.

The above analysis provides a qualitative classification that can be help to correctly choose a swirler in different technical applications. Differences in velocity profiles for turbulent and laminar regimes are significant mainly for swirlers inducing flows with slender vortex core. Nevertheless, these differences are much smaller in comparison with axial flows [27]. In the following section we study ambiguities related to the existence of the different vortex symmetry in the swirl flows with the same integral parameters. In particular, we will estimate the influence of the flow regimes on these ambiguities. In the Section 6 we will discuss how these hydrodynamic ambiguities can be projected to the heat transfer processes in pipe swirl flows.

5. Ambiguities in the swirl pipe flows with helical symmetry

In the previous work [25] we have shown that mass transfer processes in the swirl flows are not completely controlled by integral flow parameters (Reynolds number and the swirl number) but depend essentially on the type of vortex symmetry. The left-handed helical vortices generate wake-like swirl flows and increase mass

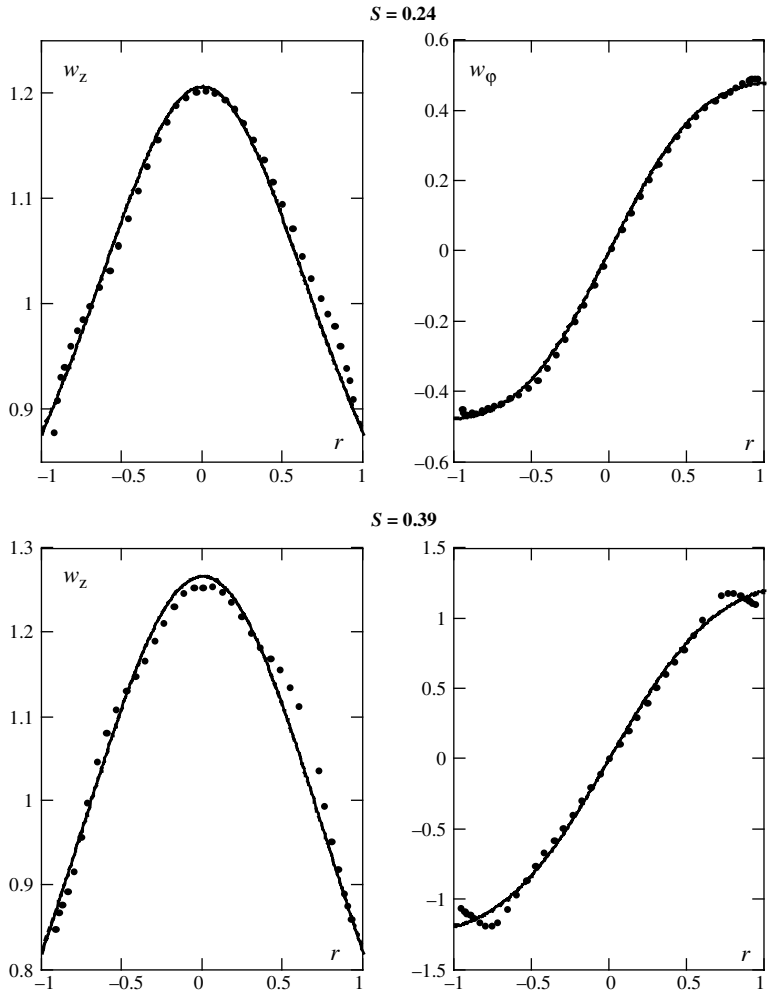

Fig. 8. Pipe swirl flow generated by rotation of the honeycomb section: solid lines—Gaussian distribution of the vorticity in the vortex core (present work); dashed lines—rational distribution of the vorticity in the vortex core (present work); points—experimental data [34] (solid and dashed lines coincide on the figure).

transfer in comparison with axial flows. The right-handed helical vortices generate jet-like swirl flows, which can decrease mass transfer. In [25], rather crude model (2.8) with the step-shape distribution of the vorticity was used to describe a swirl flow. As shown in the previous section, flow models with smooth vorticity distributions (4.2) and (4.3) are more suitable approximations for both laminar and turbulent flows. The main goal of this section is to study possible flow regimes which can arise in the pipe swirl flows under the same integral flow parameters. In other words, we study the problem of existence of the left- and right-handed helical vortices for the different vorticity distributions (4.2) or (4.3).

A swirl flow can be described by a set of integral flow parameters. We do not take into account the influence of wall friction losses. This leads one to conservation laws for five integral parameters of inviscid axisymmetric flow [18]:

flow rate

$$Q = 2\pi\rho \int_0^R w_z r \, \mathrm{d}r, \tag{5.1}$$

velocity circulation

$$G = 2\pi R w_\varphi(R), \tag{5.2}$$

axial flux of angular momentum

$$M = 2\pi\rho \int_0^R w_\varphi w_z r^2 \, \mathrm{d}r, \tag{5.3}$$

Table 1
Vortex parameters in swirl flows generated by different swirlers

Type of vortex and flow regime	Approximation of vortex core	Regime parameters			Vortex parameters				Near wall velocities	
		Re	*S*	S^*	Γ/UR^2	$2\pi l/R$	w_0/U	ε/R	W/U	V/U
Set-up with guide vane swirler [31]										
Right-handed	Model (4.2)	11 480	0.1	0.3	0.32	0.33	1.96	0.19	0.98	0.32
	Model (4.3)		0.1	0.31	0.36	0.34	1.96	0.17	0.91	0.35
Set-up with guide vane swirler [32,33]										
Right-handed	Model (4.2)	230 000	0.07	0.40	0.41	0.27	2.44	0.16	0.93	0.41
	Model (4.3)		0.07	0.43	0.47	0.28	2.45	0.15	0.82	0.46
Set-up with tangential input [4]										
Left-handed	Model (4.2)	12 500	0.21	1.1	1.35	−0.77	−0.45	0.43	1.29	1.34
	Model (4.3)		0.21	1.1	1.73	−0.76	−0.46	0.45	1.44	1.44
Set-up with axial–tangential input [34]										
Right-handed	Model (4.2)	280 000	0.25	0.34	0.45	3.4	1.13	0.46	0.99	0.45
	Model (4.3)		0.25	0.35	0.6	3.3	1.13	0.50	0.98	0.48
Left-handed	Model (4.2)	280 000	0.27	0.63	0.79	−1.38	0.58	0.44	1.15	0.78
	Model (4.3)		0.27	0.64	1.08	−1.38	0.58	0.49	1.21	0.87
Set-up with rotating honeycomb section [35]										
Right-handed	Model (4.2)	280 000	0.24	0.27	0.65	1.45	1.21	0.87	0.88	0.47
	Model (4.3)		0.24	0.27	1.05	1.45	1.21	1.00	0.88	0.47
Right-handed	Model (4.2)	280 000	0.39	0.63	1.86	2.68	1.27	0.99	0.82	1.19
	Model (4.3)		0.39	0.63	3.27	2.68	1.27	1.00	0.82	1.19

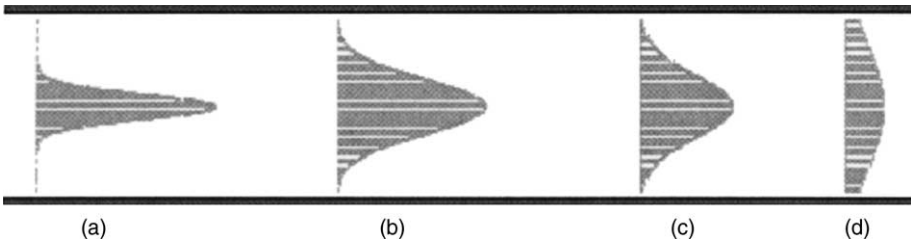

Fig. 9. Distribution of the axial vorticity in swirl pipe flows generated by the different swirlers: a—radial guide vanes [31]; b—tangential swirler [4]; c—axial–tangential inlet [34]; d—rotation of honeycomb section [35].

axial flux of momentum

$$J = 2\pi\rho \int_0^R \left(w_z^2 + \left(\int_0^r \frac{w_\varphi^2}{\sigma} \mathrm{d}\sigma + \frac{p_0}{\rho} \right) \right) r \,\mathrm{d}r, \tag{5.4}$$

axial flux of energy

$$E = 2\pi\rho \int_0^R \left(\frac{w_z^2 + w_\varphi^2}{2} + \left(\int_0^r \frac{w_\varphi^2}{\sigma} \mathrm{d}\sigma + \frac{p_0}{\rho} \right) \right) w_z r \,\mathrm{d}r. \tag{5.5}$$

Here ρ is the fluid density, and p_0 is the static pressure in the system.

The procedure presented below is valid for any type of the vorticity distribution, for example for distributions given by Eqs. (2.8), (4.2) and (4.3). Substitution of the expressions (4.1) into Eqs. (5.1)–(5.5) allows, at fixed Q, G, L, J and E, to obtain a system of five non-linear algebraic equations for the vortex structure parameters Γ, l, ε, w_0, and p_0. Equations corresponding to the conservation laws for Q, G, L and J allow to present parameters Γ, l, w_0 and p_0 as functions of the radius of the vortex core ε:

$$\begin{cases} \Gamma(\varepsilon) = \dfrac{G}{k0(\varepsilon)}, \\ l(\varepsilon) = \Gamma^2(\varepsilon) \dfrac{k1^2(\varepsilon) - \pi k2(\varepsilon)}{\pi L - Q\Gamma(\varepsilon) k1(\varepsilon)}, \\ w_0(\varepsilon) = \dfrac{Lk1(\varepsilon) - Q\Gamma(\varepsilon) k2(\varepsilon)}{\Gamma(\varepsilon)(k1^2(\varepsilon) - \pi k2(\varepsilon))}, \\ p_0(\varepsilon) = \dfrac{J}{\pi} - \dfrac{1}{\pi}\left[w_0(\varepsilon) Q - \dfrac{L}{l(\varepsilon)} + \Gamma^2(\varepsilon) k3(\varepsilon) \right]. \end{cases}$$

Substituting these expressions in the energy equation (5.5) reduces the system to one non-linear equation for the vortex radius ε:

$$w_0(\varepsilon)\left(-\frac{w_0(\varepsilon)}{2}Q+J+\frac{\Gamma^2(\varepsilon)k2(\varepsilon)}{2l^2(\varepsilon)}+\Gamma^2(\varepsilon)k4(\varepsilon)\right)-\frac{\Gamma(\varepsilon)}{l(\varepsilon)}\left(p_0(\varepsilon)k1(\varepsilon)+\frac{\Gamma^2(\varepsilon)}{l^2(\varepsilon)}k6(\varepsilon)+\Gamma^2(\varepsilon)k5(\varepsilon)\right)=E. \tag{5.6}$$

Coefficients in Eq. (5.6) depend of the vorticity distribution and are determined thus the functions f given by Eqs. (2.9), (4.2) or (4.3):

$$\begin{cases} k0(\varepsilon)=f(1,\varepsilon), \\ k1(\varepsilon)=2\pi\int_0^1 f(r,\varepsilon)r\,\mathrm{d}r, \\ k2(\varepsilon)=2\pi\int_0^1 f^2(r,\varepsilon)r\,\mathrm{d}r, \\ k3(\varepsilon)=2\pi\int_0^1\left(\int_0^r\frac{f^2(\sigma,\varepsilon)}{\sigma^3}\mathrm{d}\sigma\right)r\,\mathrm{d}r, \\ k4(\varepsilon)=\pi\int_0^1\frac{f^2(r,\varepsilon)}{r}\mathrm{d}r, \\ k5(\varepsilon)=\pi\int_0^1\frac{f^3(r,\varepsilon)}{r}\mathrm{d}r+2\pi\int_0^1\left(\int_0^r\frac{f^2(\sigma,\varepsilon)}{\sigma^3}\mathrm{d}\sigma\right)f(r,\varepsilon)r\,\mathrm{d}r, \\ k6(\varepsilon)=\pi\int_0^1 f^3(r,\varepsilon)r\,\mathrm{d}r. \end{cases}$$

Everywhere in the equations, Γ, l, ε, w_0, p_0, r imply dimensionless values $\Gamma/R*U$, l/R, ε/R, w_0/U, $p_0/\rho*U^2$, r/R, where U is a mean flow rate velocity, ρ is a liquid density. Dimensionless integrals Q, G, L, J, E imply $Q/\rho*U*R^2$, $G/R*U$, $L/\rho*U^2*R^3$, $J/\rho*U^2*R^2$, $E/\rho*U^3*R^2$.

Investigation [18] has shown that, for the flow regimes with vortex breakdown [30–33], non-linear equation (5.6) has several roots in the variation range of the parameter ε ($0\leqslant\varepsilon\leqslant 1$). Some roots correspond to a positive value of l and to the jet-like swirl flows, when the axial velocity has a maximum on the flow axis (Fig. 3c). This type of vortex structures ($l>0$) we call right-handed helical vortexes. Other roots correspond to a negative value of l and to wake-like swirl flows, when the axial velocity has a minimum on the flow axis (Fig. 3d and e). This type of vortex structures ($l<0$) we call left-handed helical vortexes. Existence of a set of roots of Eq. (5.6) means that different vortex structures may arise in the flow at the same integral flow conditions. Moreover, it explains a change in the flow regime with a transition from one vortex structure to another, experimentally observed as the vortex breakdown.

The initial regime in [31] corresponds to a flow with a jet-like profile (right helical vortex). Secondary regimes in this flow (i.e. the regimes after breakdown) correspond to a wake-like flow profile (left helical vortex). Fig. 10 shows an example of the graphic solution of Eq. (5.6) for the swirl flow investigated in [31] at $Re=11\,480$. It can be noted that for different flow models, described by the different vorticity distributions in the core, the number of roots in Eq. (5.6) varies from 2 to 4. So, all our modes predict secondary regimes with wake-like profiles, while the number of possible secondary regimes varies from 2 to 4. The existence of different secondary regimes with wake-like velocity profile has been experimentally observed (see, for example, a diagram of the vortex breakdown in [30]). It should be emphasized that different vorticity models describing either turbulent or laminar flow regimes lead to unequal number of the roots of Eq. (5.6) and thus to essential difference in secondary flows.

The quantitative differences in the flow regimes for vortex structures with vorticity distributions (4.2) or (4.3) are shown in Fig. 11. The model with a step-shaped distribution (2.8) was excluded from our consideration as being very rough a priori. We have compared experimental velocity profiles with solutions corresponding to the roots of Eq. (5.6) for both vorticity distributions. An excellent correlation was found between experimental data (symbols) and theoretical results for the initial, before breakdown, flow regime (solid line). Difference between experimental data and calculated results of the model (4.2) for the secondary flow regime (flow after breakdown, dashed lines), was found to be insignificant.

Both vortex models indicate a possible change in the helical symmetry of the axial vortex. Analysis of experimental data for the different swirlers, presented in Section 4, illustrates existence of the right- and left-handed vortex structures in swirl flows without vortex breakdowns (see Figs. 6–8 and Table 1). It this section we have shown that, under the same integral parameters (5.1)–(5.5), different vortex structures may appear in the

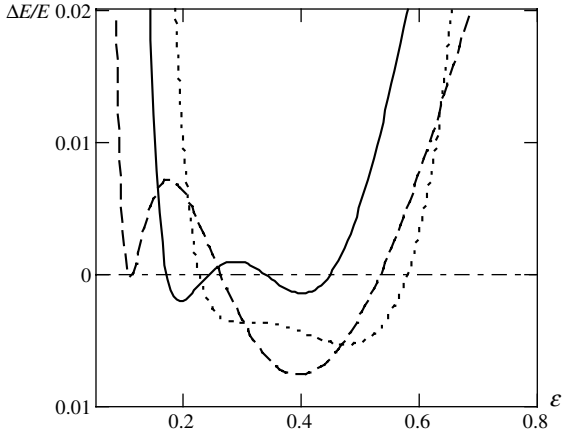

Fig. 10. Graphical solutions of Eq. (5.6) for different vorticity distributions in the vortex core obtained for the flow regime with vortex breakdown [31] at $Re=11\,480$: solid line—Gaussian distribution of the vorticity in the vortex core [18]; dot line—rational distribution of the vorticity in the vortex core [18]; dashed line—step-shaped distribution of the vorticity in the vortex core [18].

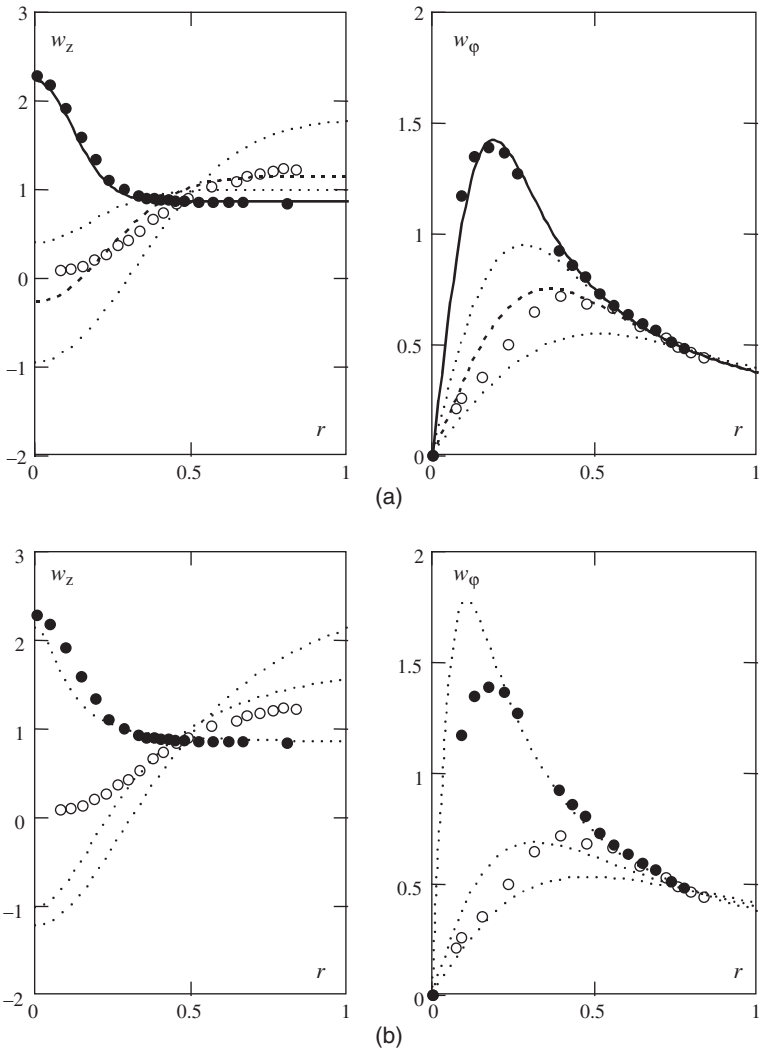

Fig. 11. Comparison of experimental and calculated axial w_z and tangential w_φ velocity profiles: (a) Gaussian vorticity distribution, Eq. (4.2); (b) rational vorticity distribution, Eq. (4.3). Symbols—experimental data of [31] at $Re = 11\,480$; solid line—calculations (present work) of the velocity profile for the initial flow regime (before breakdown); dashed line—calculations (present work) of the velocity profile for the secondary flow regime (after breakdown); dot lines—calculations (present work) of the velocity profile for all possible flow regimes corresponding to Eq. (5.6).

same swirl flow. Moreover, transition from one vortex structure to another is also possible in a flow in a cylindrical tube (for example, in the flows with vortex breakdown, Fig. 11). The existence of the ambiguities in the swirl flows means that the set of integral flow parameters (5.1)–(5.5) is, in general, insufficient for classification of swirling pipe flows. As a consequence, flows having the same Reynolds number Eq. (2.2) and the same swirl number (2.3), but with different helical symmetry or with different distribution of the vorticity field, will differ from the heat (or mass) transfer point of view. This effect will be quantitatively analyzed in the following section.

6. Discussion and conclusions

The main goal of this paper is to study one of the mechanisms of heat transfer enhancement in the pipe swirl flow related to the increase of the axial velocity near the wall. Our study shows that traditional empirical correlations for swirl flows, described by Eqs. (2.4)–(2.7) are, in general, insufficient. Indeed, two types of vortex structures, with left-handed and right-handed helical symmetry, can exist in the swirl flows with the same integral characteristics. Two major factors of the velocity augmentation have been identified: (i) formation of the swirl flow with left-handed helical vortex;

Table 2
Vortex parameters in swirl flow with vortex breakdown [31]

	Integral flow parameters								
	G/RU	$Q/\rho UR^2$	$M/\rho U^2R^3$	$J/\rho U^2R^2$	$E/\rho U^3R^2$				
	0.37	3.1	1.0	21.4	18.6				
Vortex type	Vortex parameters								
	$\frac{a}{R}$	$\frac{\Gamma}{UR}$	$\frac{2\pi l}{R}$	$\frac{w_0}{U}$	$\frac{p_0}{\rho U^2}$	$\frac{V}{U}$	$\frac{W}{U}$	$\left(\frac{Re_W}{Re_U}\right)^{1/2}$	$\left(\frac{Re_{(V,W)}}{Re_U}\right)^{1/2}$
Approximation of vortex core by Gaussian distribution of the vorticity (4.2)									
Right helix	*0.17*	*0.37*	*0.27*	*2.23*	*0.00*	*0.37*	*0.86*	*0.93*	*0.96*
Left helix	0.25	0.37	−0.63	0.39	1.89	0.37	1.01	1.00	1.01
Left helix	*0.32*	*0.37*	*−0.26*	*−0.27*	*2.32*	*0.37*	*1.15*	*1.07*	*1.09*
Left helix	0.46	0.39	−0.14	−0.96	2.32	0.39	1.76	1.32	1.34
Approximation of vortex core by rational distribution of the vorticity (4.3)									
Right helix	0.11	0.38	0.29	2.13	−2.79	0.37	0.84	0.92	0.95
Left helix	0.31	0.43	−0.15	−1.02	2.14	0.39	1.54	1.24	1.26
Left helix	0.48	0.51	−0.12	−1.23	2.18	0.41	2.12	1.46	1.46

(ii) modification of the velocity profile due to the different vorticity distribution in the vortex core, see Fig. 11.

To support these conclusions, we have used Eqs. (3.6) and (3.7) to calculate hydrodynamic parameters (relative Reynolds numbers) which determine heat transfer enhancement. Table 2 presents these parameters for different vortices. The vortex parameters were calculated for seven vortex structures (see Fig. 11), which have the same integral flow characteristics corresponding to the real swirl [31].

Left-handed helical vortexes generate wake-like swirl flows, while right-handed vortex structures generate jet-like swirl flows. Estimations show (Table 2) that, under the same integral flow characteristics, change of the vortex symmetry can increase heat transfer at least at 54% (in case of the rational distribution). It can be noted that wall heat flux is more important for all left-handed vortices in comparison with the right-handed vortices under same flow characteristics. In all these cases, wall heat flux in the swirl flows with left-handed vortices is greater than in the axial flow. On the other hand, right-handed vortices decrease the wall heat flux in comparison with the developing axial flow having the same Re number.

Another result deals with the influence of the vorticity distribution on heat transfer. We note that, under the same integral characteristics, different left-handed helical vortices give different heat enhancement in comparison with the axial flow. The most important enhancement corresponds to the rational distribution of the vorticity (about 46%). As is shown above, rational distribution is the most suitable approximation for turbulent flows. Maximum enhancement that was obtained using Gaussian distribution is 32%. This distribution is more appropriate approximation for laminar swirl flows.

From engineering point of view, our study leads to three important conclusions:

(i) In order to increase the wall heat flux in vortex devices, it is preferable to realize left-handed vortex structures.
(ii) By using of a suitable vortex device, it is possible to modify vorticity distribution in the flow core and to increase heat enhancement under the same integral flow characteristics. It is important to look for the devices that generate smooth distribution of the vorticity in the vortex core.
(iii) Spontaneous transition from one to another type of vortex symmetry is possible in the vortex devices, even if all integral flow parameters are well controlled. The transition to another vortex symmetry can provoke an important change of heat transfer characteristics.

Acknowledgements

This work was carried out in the Laboratory of Heat Studies of Poitiers: "LET—UMR CNRS no 6608". The authors wish to thank the University of Poitiers and the Ministry of High Education of France who made this work possible by granting to one of them the position of visiting professor. This work was partially supported by the French pluri-formation program "Near interface transfer on micro-scale level" (The Ministry of High Education), by INTAS (Grant No. 00-00232) and by the Russian Foundation for Basic Research (Grant No. 01-01-00899).

References

[1] A. Gupta, D.G. Lilley, N. Syred, Swirl Flows, Abacus Press, Cambridge, 1984.

[2] A. Ivanova, Increasing the rate of heat transfer in a round air-cooled tube, in: Proceedings Second All-Soviet Union Conference on Heat and Mass Transfer, Minsk, vol. 1, 1964, pp. 243–250.
[3] E.G. Narazhnyy, A.V. Sudarev, Local heat transfer in air flowing in tubes with a turbulence promoter at the inlet, Heat Transfer—Soviet Res. 3 (2) (1971) 62–66.
[4] F. Chang, V.K. Dhir, Mechanisms of heat transfer enhancement and slow decay of swirl in tubes using tangential injection, Int. J. Heat Fluid Flow 16 (2) (1995) 78–87.
[5] F.A. Blum, L.R. Oliver, Heat transfer in decaying vortex system, ASME Paper no. 66-WA/HT-62, 1975.
[6] N.H. Zaherzade, B.S. Jagadish, Heat transfer in decaying swirl flow, Int. J. Heat Mass Transfer 18 (1975) 941–944.
[7] M. Yilmaz, S. Yapici, O. Jomakli, O.N. Sara, Energy correlation of heat transfer and enhancement efficiency in decaying swirl flow, Heat Mass Transfer 38 (2002) 351–358.
[8] A.H. Algifri, R.K. Bhardwaj, Y.V.N. Rao, Heat transfer in a turbulent decaying swirl flow in a circular pipe, Int. J. Heat Mass Transfer 19 (1980) 613–620.
[9] P. Legentilhomme, J. Legrand, The effects of inlet conditions on mass transfer in annular swirling decaying flow, Int. J. Heat Mass Transfer 35 (1991) 1281–1291.
[10] M.S. De Sa, E. Shoukry, I. Soegiarto, Mass transfer enhancement in the entrance region for axial and swirling annular flow, Canad. J. Chem. Eng. 69 (1991) 294–299.
[11] S. Yapici, M.A. Patrick, A.A. Wragg, Electrochemical study of mass transfer in decaying annular swirl flow. Part 2: correlation of mass transfer data, J. Appl. Electrochem. 25 (1995) 15–22.
[12] S. Yapici, G. Yazici, C. Ozmetin, H. Ersahan, Mass transfer to local electrodes at wall and wall friction factor in decaying turbulent swirl flow, Int. J. Heat Mass Transfer 40 (1997) 2775–2783.
[13] D.R. Weske, G.Ye. Sturov, Experimental study of turbulent swirled flows in a cylindrical tube, Fluid Mech.—Soviet Res. 3 (1974) 77–82.
[14] S.V. Alekseenko, V.L. Okulov, Swirl flow in technical applications (review), Thermophys. Aeromechan. 3 (2) (1996) 97–128.
[15] S.V. Alekseenko, P.A. Kuibin, V.L. Okulov, S.I. Shtork, Helical vortices in swirl flow, J. Fluid Mech. 382 (1999) 195–243.
[16] V.L. Okulov, The transition from the right helical symmetry to the left symmetry during vortex breakdown, Tech. Phys. Lett. 22 (10) (1996) 798–800.
[17] T. Murakhtina, V.L. Okulov, Changes in topology and symmetry of vorticity field during the turbulent vortex breakdown, Tech. Phys. Lett. 26 (10) (2000) 798–800.
[18] T. Murakhtina, V.L. Okulov, Influence of distribution of vorticity in core of swirl flow on the description of spontaneous change in flow regimes, Thermophys. Aeromech. 7 (1) (2000) 63–68.
[19] R.F. Lopina, A.E. Bergles, Heat transfer and pressure drop in tape-generated swirl flow of single-phase water, ASME J. Heat Transfer 91 (1969) 434–442.
[20] A. Durmus, Heat transfer and exergy loss in a concentric heat exchanger with snail entrance, Int. Comm. Heat Mass Transfer 29 (3) (2002) 303–312.
[21] A.N. Algifri, R.K. Bhardwaj, Prediction of the heat transfer for decaying turbulent swirl flow in a tube, Int. J. Heat Mass Transfer 28 (1985) 1637–1643.
[22] S.Yu. Spotar', V.I. Terekhov, Two spontaneously alternating regimes of vortex flow above a plane, J. Appl. Mech. Tech. Phys. 2 (1987) 227–228.
[23] E.P. Volchkov, N.A. Dvornikov, V.P. Lebedev, V.V. Lukashov, The investigations of vortex chamber aerodynamics, in: Proceedings of III Russian–Korean International Symposium on Science and Technology, Novosibirsk, vol. 1, 1999, pp. 40–43.
[24] P.A. Kuibin, V.L. Okulov, One-dimensional solutions for a flow with a helical symmetry, Thermophys. Aeromech. 3 (4) (1996) 335–339.
[25] S.A. Martemianov, V.L. Okulov, Mass transfer ambiguities in swirling pipe flows, J. Appl. Electrochem. 32 (2002) 25–34.
[26] R. Razgaitis, J.P. Holman, A survey of heat transfer in confined swirl flows, Heat Mass Transfer Proc. 2 (1976) 831–866.
[27] H. Schlichting, Boundary-Layer Theory, seventh ed., McGraw-Hill, 1979.
[28] W.M. Rohsenow, J.P. Hartnett, Y.I. Cho (Eds.), Handbook of Heat Transfer, McGraw-Hill, 1998.
[29] F. Kreith, O.K. Sonju, The decay of a turbulent swirl in a pipe, J. Fluid Mech. 22 (1965) 257–271.
[30] J.H. Faler, S. Leibovich, Disrupted states of vortex flow and vortex breakdown, Phys. Fluids 20 (1977) 1385–1399.
[31] A.K. Garg, S. Leibovich, Spectral characteristics of vortex breakdown flow fields, Phys. Fluids 22 (1979) 2053–2064.
[32] T. Sarpkaya, F. Novak, Turbulent vortex breakdown at high Reynolds numbers, in: Proceedings 37th AIAA Aerospace Meeting and Exhibition, 1999, AIAA 99-0135, pp. 1–18.
[33] T. Sarpkaya, F. Novak, Turbulent vortex breakdown: experiments in tube at high Reynolds numbers, in: E. Krause, K. Gersten (Eds.), Proceedings IUTAM-Symposium on Dynamics of Slender Vortices, Fluid Mechanics and its Applications, vol. 44, 1998, pp. 287–296.
[34] O.G. Dahlhaug, Thesis of Doctor Engineer degree, NTNU, Trondheim, Norway, 1997.
[35] M. Schmidts, V. Vasanta Ram, Turbulence characteristics in pipe flow with swirl, in: S. Dopazo (Ed.), Proceedings of ETC-8 'Advance in Turbulence', Barcelona, vol. 8, 2000, pp. 121–124.